BNL-228363-2025-JAAM

Earth-Abundant Manganese Nitride Catalysts for Mild-Condition Ammonia Synthesis

W. Qu, L. Ma

To be published in "ACS Catalysis"

March 2025

Photon Sciences

Brookhaven National Laboratory

U.S. Department of Energy

USDOE Office of Science (SC), Basic Energy Sciences (BES). Scientific User Facilities (SUF)

DISCLAIMER

Earth-abundant manganese nitride catalysts for mild-condition ammonia synthesis

Weiye Qu,[†,‡] Pranav Roy,[†,‡] Canhui Wang,[†] Lu Ma,[▽] Fan Bu,[†] Xinsui Zhang,[†] Zimin He,[†] Michael Tsapatsis,[†,§] Brandon C. Bukowski,[*,†] Chao Wang[*,†]

[†]Department of Chemical and Biomolecular Engineering, Johns Hopkins University, Baltimore, MD 21218, USA.
[▽]National Synchrotron Light Source, Brookhaven National Laboratory, Upton, NY 11973, USA.
[§]Applied Physics Laboratory, Johns Hopkins University, 11100 Johns Hopkins Road, Laurel, MD 20723, USA.

KEYWORDS: Ammonia Synthesis, Nitrides, Heterogeneous catalysis, Nitrogen vacancy, Associative mechanism

ABSTRACT: Developing advanced catalytic materials for mild-condition ammonia (NH_3) synthesis is essential for improving the energy efficiency of this key industrial process. Here, we report a ζ-phase manganese-nitride ($MnN_{0.43}$) catalyst for low-temperature NH_3 synthesis. The as-synthesized $MnN_{0.43}$ catalyst is protected by a carbon shell, allowing for storage and processing of the air-sensitive metal nitride under ambient conditions. After activation *in situ*, the $MnN_{0.43}$ catalyst exhibits high activity for NH_3 synthesis at 250-350 °C, surpassing the conventional noble metal based Ru/MgO catalyst. A combination of kinetic, chemisorption and computational studies indicate that a nitrogen vacancy-mediated associative mechanism accounts for the catalytic enhancements. Our work highlights the great potential of earth-abundant transition metal nitrides for catalyzing mild-condition NH_3 synthesis.

INTRODUCTION

As a primary feedstock for fertilizers and nitrogen-containing chemicals,[1-2] as well as a promising carbon-free fuel and hydrogen carrier,[3-4] NH_3 plays a crucial role in modern chemical industry. Up to now, NH_3 is primarily synthesized via the Haber-Bosch process,[5] which requires harsh conditions (150-200 bar, 400-500 °C) due to the significant energy required to cleave the N ≡ N triple bond (945 kJ mol^{-1}).[6] This process is highly energy-intensive, accounting for about 1-2% of global energy consumption and CO_2 emissions.[7-9] Advanced catalysts that can catalyze NH_3 syntheses under mild conditions are thus pursued to reduce the energy consumption for the Haber-Bosch process.[9-11]

Ruthenium (Ru) is known as the most active metal for NH_3 synthesis.[12] Early studies showed that supported Ru nanoparticles of ~2 nm preferentially expose B_5 type step sites, which are particularly active for dissociative adsorption of N_2.[13-14] However, the high cost and scarcity of Ru hinder its industrial applications. More recently, rare earth metal nitrides such as CeN and LaN have been reported to be promising NH_3 synthesis catalysts.[10,15-16] It is suggested that the nitrogen vacancies (N_V) present on such metal nitride surfaces can readily adsorb N_2 in linear configurations and the activation of N_2 starts with hydrogenation of the tailing nitrogen. The preceding hydrogenation prior to breaking the nitrogen-nitrogen bonding allows for the reaction to proceed via an associative pathway.[17] This pathway bypasses the direct dissociation of N≡N bond as in the case for Ru, giving rise to lower energy barriers and reducing the temperature (and thereby pressure) needed to drive the Haber-Bosch process. However, such rare earth metal nitride catalysts also involve critical materials. In addition, they are sensitive to air and humidity, imposing challenges for synthesis and processing in practical implementations.[10,15-16]

In our search for earth-abundant transition metal nitrides as NH_3 synthesis catalysts, manganese nitrides (Mn_xN_y) stand out as promising candidates. Mn_xN_y exist in multiple stable and metastable phases, including MnN (rocksalt), $MnN_{0.43}$ (*hcp*), Mn_3N_2 (distorted rocksalt), and Mn_4N (anti-perovskite), etc.[18] They have previously been studied as N carrier for NH_3 production via chemical looping.[19-21] For example, Mn_4N promoted by alkali and alkaline earth metal hydrides have been reported to exhibit high NH_3 production rates at 300-400 °C.[22] Among the various Mn_xN_y, ζ-phase manganese nitrides, including Mn_2N, Mn_5N_2 and $MnN_{0.43}$,[23] have attracted our particular attention. Their variable valence of manganese can accommodate high densities of nitrogen vacancies,[24] making them promising candidates for catalyzing nitrogen chemistries. It has been reported that the nitrogen vacancy formation energy on Mn_2N surfaces is as low as 0.50 eV via hydrogenative desorption, making it facile to produce NH_3 after nitrification at high temperatures.[20] However, studies of Mn_xN_y in catalytic NH_3 synthesis have been limited to date. One plausible cause could be their high sensitivity to air and moisture, similar to those rare earth metal nitrides, which has made it difficult to assess the intrinsic catalytic performance of such materials.[25-26]

We report here ζ-phase $MnN_{0.43}$ as catalysts for NH_3 synthesis. Freestanding $MnN_{0.43}$ were synthesized by co-pyrolyzing manganese acetate and urea in N_2 (**Scheme 1**).[27] The obtained catalyst was characterized by combining transmission electron microscope (TEM), X-ray diffraction

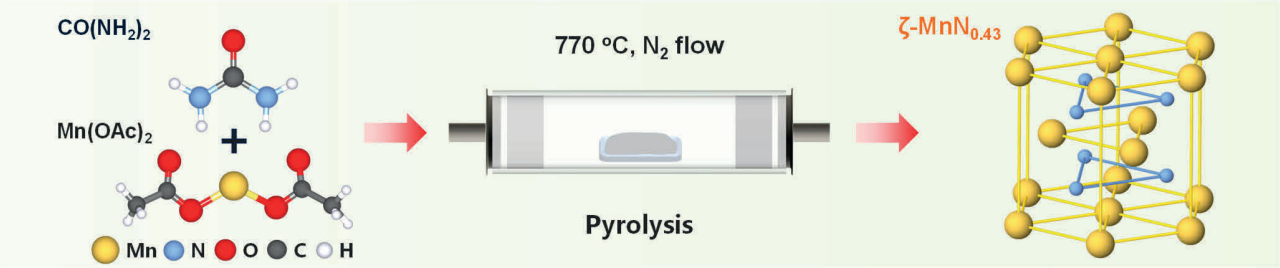

Scheme 1. Schematic diagram of catalyst synthesis.

(XRD) and X-ray photoelectron spectroscopy (XPS). After activation *in situ*, N_2-to-NH_3 conversion was measured at 250–350°C and 10 bar using a plug-flow reactor (Figure S1).[28] Kinetic studies, chemisorption analysis and computational simulation were combined to probe the active sites and reaction pathways, based on which the catalytic mechanisms for low-temperature N_2 activation were interpreted.

MATERIALS AND METHODS

The $MnN_{0.43}$ catalyst was synthesized using a sol-gel pyrolysis method (**Scheme 1**). Typically, 1.0 g of manganese acetate tetrahydrate was dissolved in 5.0 mL of methanol with stirring. After the formation of a transparent solution, 1.8 g of urea was added. The obtained solution was then transferred into a crucible and pyrolyzed at 770 °C under nitrogen for 3 h to form $Mn_{0.43}N$. Material characterization, catalytic evaluation, and theoretical calculations are detailed in the Supporting Information.

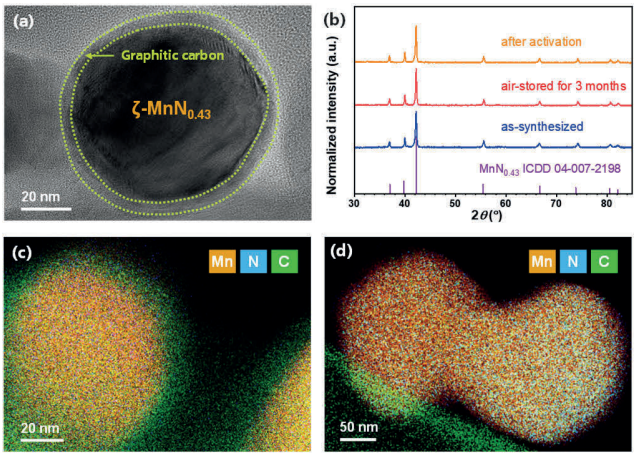

Figure 1. (a) HRTEM images of $MnN_{0.43}$@C. (b) XRD patterns of as-synthesized, air-stored, and activated samples. (c, d) EDX mapping images of $MnN_{0.43}$@C and $MnN_{0.43}$.

RESULTS AND DISCUSSION

The as-synthesized $MnN_{0.43}$ catalyst primarily exhibits a pseudospherical morphology with particle sizes ranging from ~30 to ~100 nm (Figure S2). High-resolution TEM (HRTEM) imaging reveals that the as-synthesized catalysts have a core-shell nanostructure (**Figure 1a**). The core nanocrystal displays lattice fringes with spacing of 2.15 Å (Figure S2), which can be attributed to the (111) crystal planes of ζ-phase $MnN_{0.43}$. XRD patterns exhibit primary peaks at 36.9°, 39.9° and 42.2°, which can be assigned to the (110), (002) and (111) peaks of ζ-phase $MnN_{0.43}$ (**Figure 1b**). The crystal size is estimated to be ~66 nm from the XRD pattern using the Sherrier equation, which is also in line with the TEM results. The metal nitride nanoparticles are surrounded by a distinct shell of lower electron contrast, with the shell thickness measured to be ~5 nm (**Figure 1a**). The lattice fringe exhibits an interlayer spacing of 3.40 Å (Figure S2), corresponding to the (002) plane of graphite. Energy-dispersive X-ray (EDX) further indicates that C is concentrated in the outer shell, while Mn and N are uniformly distributed within the core particle (**Figures 1c** and S3). Thus, the as-synthesized catalyst is denoted as $MnN_{0.43}$@C.

Normally, manganese nitride is easily oxidized to manganese oxide when exposed to air.[26,29] In the $MnN_{0.43}$@C catalyst, the graphite shell is able to protect the metal nitride core from oxidation post the synthesis. **Figure 1c** shows a catalyst after 3 months of storage in air. No oblivious structural change was observed. No manganese oxide phase was detected from XRD analysis either (**Figure 1b**). The $MnN_{0.43}$@C catalyst was pretreated at 500 °C for 0.5 h in a NH_3 synthesis atmosphere (25%N_2–75%H_2, 10 bar) and then processed under inert atmosphere for further characterization. As shown in **Figure 1d** (also Figures S4 and S5), the graphitic shell was completely removed after pretreatment and the metal nitride nanoparticles became exposed. The stabilization in air plus facile *in situ* activation is considered to be an advantage of the $MnN_{0.43}$@C catalyst for industrial practice, where storage and installation/replacement of catalysts are usually done under ambient conditions.[30] The activated catalyst has a N/Mn element ratio of ~0.47 (Table S1), close to the expectation for $MnN_{0.43}$.

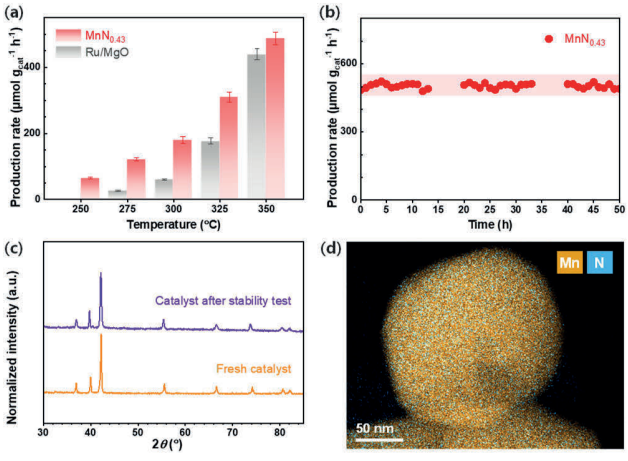

Figure 2. (a) NH_3 production rate as a function of temperature over $MnN_{0.43}$ and reference 5 wt% Ru/MgO. Reaction conditions: 25% N_2, 75% H_2, WHSV = 30,000 ml g_{cat}^{-1} h^{-1}, and 10 bar. (b) Stability test over $MnN_{0.43}$ at 350 °C and 10 bar. (c) XRD patterns of fresh catalyst and used catalyst. (d) EDX mapping image of $MnN_{0.43}$ after stability test.

Catalytic performance of the activated $MnN_{0.43}$ catalyst for NH_3 synthesis was evaluated using a 25% N_2–75% H_2 feed under a weight hourly space velocity (WHSV) of 30,000 mL g^{-1} h^{-1}. Accuracy of the low-temperature activity was verified through quantitative isotope-labeled $^{15}N_2$ experiments coupled with ^1H NMR analysis (Figure S6).[31] **Figure 2a** shows the NH_3 production rates at 10 bar as a function of reaction temperature. The $MnN_{0.43}$ catalyst exhibits NH_3 synthesis activity in the temperature range of 250–350°C, with the NH_3 yield increasing from 65 μmol NH_3 g_{cat}^{-1} h^{-1} at 250 °C to 488 μmol NH_3 g_{cat}^{-1} h^{-1} at 350°C. The catalytic performance of $MnN_{0.43}$ represents one of the best as compared to the other metal nitride catalysts reported in the literature (Table S2). It is also superior to the Ru control (5 wt% Ru/MgO) measured in the same temperature range, demonstrating an improvement factor of >3 below 300 °C (**Figure 2a**). Notably, the $MnN_{0.43}$@C sample stored in air for over 3 months shows nearly identical activity to the freshly prepared sample after activation (Figure S7), confirming its advantage for on-shelf storage and practical handling.

After demonstrating catalytic enhancement, we examine the stability of the $MnN_{0.43}$ catalyst under the NH_3 synthesis reaction conditions. **Figure 2b** describes the NH_3 production rate recorded during a continuous operation at 350°C. Change in catalytic activity is <1% after 50 hours of reaction. XRD analysis (with sample sealed using Kapton film in Ar glove box) after the stability test found no change to the crystal structure (**Figure 2c**). Element mapping based on EDX also confirmed the uniform distribution of Mn and N in the tested catalyst (**Figure 2d**; also see Figure S8). The N/Mn element ratio was also found to be consistent (Table S1), indicating no N loss from the catalyst throughout the reaction.

Kinetic studies were conducted to explore the catalytic mechanism of $MnN_{0.43}$. As shown in **Figure 3a**, the apparent activation energy (E_a) of $MnN_{0.43}$ is found to be only 53.4 kJ mol^{-1}, which is significantly lower than that of Ru/MgO (107.7 kJ mol^{-1}). Notably, it is also among the lowest E_a values reported in the literature (Table S3). The NH_3 synthesis reaction rate with $MnN_{0.43}$ exhibits a N_2 reaction order of $\beta(N_2) \approx 0.61$ (**Figure 3b**), which is also notably lower than that (1.2) recorded for Ru/MgO. This is distinct from conventional Fe and Ru-based catalysts, for which the N_2 reaction order being close to 1 is indicative of having N≡N dissociation as the rate-determining step.[32-34] It also signifies facile activation of N_2 on $MnN_{0.43}$ through an alternative mechanism to direct N_2 dissociation. The $MnN_{0.43}$ catalyst gives a H_2 reaction order $\beta(H_2) \approx 1.7$, in contrast to −0.67 for Ru/MgO (**Figure 3c**). The negative value of $\beta(H_2)$ is a typical feature of H_2 poisoning on Ru-based catalysts due to their strong binding to hydrogen.[33,35] The positive value observed for $MnN_{0.43}$ suggests that the reaction is no longer subjected to hydrogen poisoning, which is further supported by the absence of H_2 desorption signals from the temperature-programmed desorption of hydrogen (H_2-TPD, Figure S9) measurements post the catalytic studies. The latter finding also rules out the possibility of hydrogen storage mechanisms for the positive H_2 order (as seen, e.g., in electride catalysts[36]). Instead, the large H_2 order (1.7) is indicative of a hydrogenation step being the rate-limiting factor. The NH_3 reaction order (−1.5) measured on $MnN_{0.43}$ is similar to those reported for CeN (-1.6) and industrial Fe-based catalysts (ca. −1.5) (Figure S10), implying strong binding of NH_x (x = 1, 2 or 3) on these catalysts.[15,34]

The above kinetic features of $MnN_{0.43}$, including low E_a, small N_2 order and large positive H_2 order, all point to the associative mechanism that proceeds with hydrogenation of N_2 prior to nitrogen-nitrogen bond cleavage. The associative mechanism was further supported by the N_2 isotopic exchange reaction (N_2-IER) measurements, from which N_2 dissociation was found to be unlikely on $MnN_{0.43}$ in the temperature range investigated for NH_3 synthesis (250-350 °C) (Figure S11). Inspired by the previous studies of nitrogen vacancies on rare earth metal nitrides for N_2 activation,[10,15-16] we have used XPS to probe such defect sites on $MnN_{0.43}$ (Figures S12 and S13). The Mn $2p_{3/2}$ band in the XPS spectrum are deconvoluted into two peaks at 641.1 and 642.1 eV, which are assigned to the Mn atoms adjacent to N vacancies (defined as Mn_A) and surrounded by N atoms (defined as Mn_B), respectively.[37-38] Therefore, the peak at 641.1 eV is indicative of the presence of N_v on the $MnN_{0.43}$ catalyst. The N 1*s* peak in the XPS spectrum can be deconvoluted into three peaks at 397.8, 399.1, and 401.1 eV. The peaks at 397.8 and 401.1 eV can be assigned to lattice N from manganese nitride and graphitic N from the shell,[39-40] respectively, while the shoulder peak at 399.1 eV to N_v.[38,41-42] To exclude the interference of N in the graphite shell, we further performed XPS analysis on the activated $MnN_{0.43}$ sample (Figure S13). After activation, the graphite N peak at 401.1 eV disappeared, while the shoulder peak at 399.3 eV remained, ruling out the possibility of pyrrolic and pyridinic N.[40,43] The XPS results thus confirmed the presence of nitrogen vacancies on the $MnN_{0.43}$ catalyst. Furthermore, Mn *K*-edge X-ray absorption spectra (XAS) analysis[44-45] reveals that the average valence state of Mn in $MnN_{0.43}$ is ~1.2 (Figure S14), which is in line with its stoichiometry.

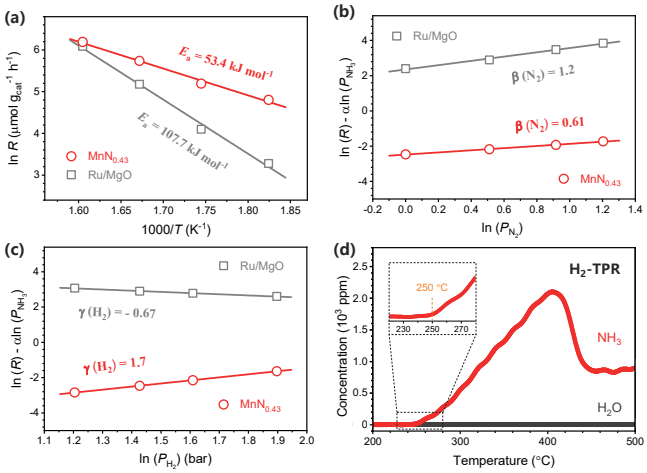

Figure 3. (a) Arrhenius-type plots for NH_3 synthesis over $MnN_{0.43}$ and Ru/MgO with the related activation energies. (b) N_2 and (c) H_2 reaction orders of $MnN_{0.43}$ and 5wt% Ru/MgO at 350 °C. (d) H_2-TPR profile of $MnN_{0.43}$ under H_2 pressure of 10 bar with WHSV of 30,000 ml g_{cat}^{-1} h^{-1}.

To examine the surface properties, we further measured temperature-programmed desorption of nitrogen (N_2-TPD) on the activated $MnN_{0.43}$ catalyst (Figure S15). The N_2-TPD profile exhibits a desorption peak at ~370 °C, which can be attributed to the intermediate N species from the NH_3 synthesis reaction associated with the surface Nv sites.[15-16] The shoulder peak at 500–600 °C and the rising band above 600 °C correspond to the desorption of surface lattice N and bulk lattice N, respectively.[16] The formation of

N_v can take place at lower temperatures in the presence of H_2. Temperature-programmed reaction with hydrogen (H_2-TPR) measurements on the $MnN_{0.43}$ catalyst recorded onset of NH_3 release at 250 °C (**Figure 3d**). This finding is in line with the observation of ammonia synthesis reactivity starting from 250 °C and is comparable to recently reported state-of-the-art rare earth metal nitride-based catalysts (e.g., 250 °C for Ni/LaN and 220 °C for Ni/CeN.[10,15] Notably, the $MnN_{0.43}$ surface itself can activate H_2 at such low temperatures, distinct from those rare earth metal nitride-based catalysts that need the presence of additional transition metal particles (e.g., Ni) on the surface as H_2 activation sites.

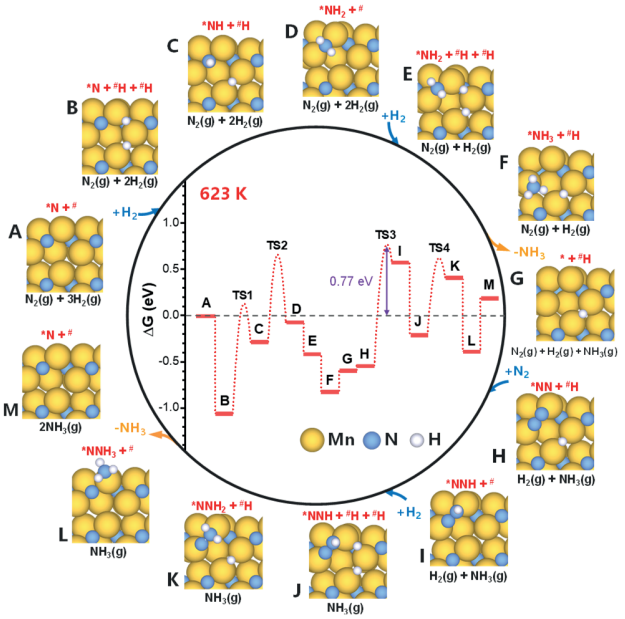

Figure 4. Gibbs free energy profile of the reaction path for NH_3 synthesis on $MnN_{0.43}$ ($1\bar{1}0$) surface at 350 °C. The surface N vacancy site and Mn-Mn bridge sites are represented by "*" and "#" respectively.

To gain molecular-level insights into the catalytic mechanism of $MnN_{0.43}$ for NH_3 synthesis, density functional theory (DFT) calculations were performed to construct a free energy profile at 350 °C for the associative mechanism (**Figure 4**; Figures S16-S23 and Tables S4-5). We found that H_2 undergoes dissociative adsorption on the Mn metal top site (**A→B**, via negligible energy barrier), with each H atom occupying an Mn-Mn bridge site. The formation of a surface N_v can proceed via sequential hydrogenation of N on the nitride surface. First hydrogenation of the lattice N occurs via migration of the closer H atom to the lattice N (**B→C**), forming *NH with an intrinsic activation energy barrier of 1.19 eV (Figure S18). This is followed by the second hydrogenation via migration of the farther H atom to *NH (**C→D**), forming $*NH_2$, which occupies the Mn-Mn bridge site due to more steric freedom. The intrinsic activation energy barrier of the second H migration is 0.94 eV (Figure S19). The dissociative adsorption of the second H_2 on the surface occurs similarly to that of the first H_2, with H atoms occupying two Mn-Mn bridge sites (**D→E**). The third hydrogenation step, occurring via migration of the closest H atom to $*NH_2$ to form $*NH_3$ spontaneously (**E→F**), proceeds through a negligible intrinsic activation energy barrier. Thus, the first half of the reaction cycle, ending in the release of one NH_3 molecule and the formation of a surface N_v (**F→G**), is exothermic by 0.59 eV, supporting the favorable formation of surface N_v in the presence of H_2, consistent with the N_2-TPD (Figure S15) and H_2-TPR (**Figure 3d**) results.

Next, the N_2 molecule adsorbs at the formed N_v in a Mn-Mn bridge-site configuration (**G→H**), differing from the linear adsorption configuration reported at N_v on rare earth metal surfaces.[10,15-16] This distinct *NN configuration may be attributed to the unique surface structure of the $MnN_{0.43}$ catalyst. In the rock salt structures of LaN, CeN, and YN, surface N_v is surrounded by four metal atoms, forming a four-fold hollow site that could facilitate end-on adsorption of N_2. While on the $MnN_{0.43}$ surface, N_v is surrounded by only two surface Mn atoms, making bridge-site adsorption of N_2 more favorable. Direct cleavage of the N≡N bond in *NN has a high intrinsic activation energy barrier of 4.22 eV on the $MnN_{0.43}$ surface (Figure S20), making it unlikely for the reaction to go through the dissociative mechanism,[14] in line with N_2-IER (Figure S11) results.

Our simulation shows that activation of *NN on the $MnN_{0.43}$ surface can proceed with migration of the remaining H atom (from **E→F→G**) and hydrogenation of *NN to form a *NNH moiety (**H→I**). This step has an intrinsic activation energy barrier of 1.31 eV (Figure S21). The nitrogen-nitrogen bond length increases from 1.21 Å for *NN to 1.29 Å for *NNH, implying weakened bonding due to hydrogenation. The hydrogenation cycle is continued via the dissociative adsorption of a third H_2 molecule onto the Mn-Mn bridge sites (**I→J**). The migration of the closer H atom (on the neighboring Mn-Mn bridge site) to the *NNH structure to form $*NNH_2$ (**J→K**) is endothermic by 0.41 eV, proceeding via an intrinsic activation energy barrier of 0.83 eV (Figure S22). The hydrogenation of *NNH to $*NNH_2$ further increases the nitrogen-nitrogen bond length from 1.29 Å to 1.41 Å, making the bond weak enough that the NH_2 adsorbs weakly onto the surface Mn atom. The final hydrogenation step, occurring via migration of the remaining H atom to $*NNH_2$ to form $*NNH_3$ (**K→L**), proceeds through a negligible intrinsic activation energy barrier. The N-N bond in $*NNH_3$ breaks spontaneously to release NH_3, leaving a N atom to replenish the surface N_v (**L→M**) and close the reaction cycle. Notably, the apparent activation energy barrier of the reaction at 350 °C is associated with the formation of *NNH via the hydrogenation of *NN, with a value of 0.77 eV (roughly 74.3 kJ mol^{-1}), in reasonable agreement with the experimentally measured E_a of 53.4 kJ mol^{-1}.

In summary, we have developed an efficient NH_3 synthesis catalyst based on earth-abundant manganese nitride. The as-synthesized catalyst features a core-shell structure, with the carbon layer protecting the $MnN_{0.43}$ core from oxidation, making it compatible for storage and processing under ambient conditions. After *in situ* activation, the $MnN_{0.43}$ catalyst demonstrates enhanced activity compared to Ru/MgO at 250–350°C, along with great stability. A combination of kinetic, chemisorption and computational simulation suggests that an associative pathway mediated by nitrogen vacancies accounts for the mild-condition reactivity. Our work sheds light on earth-abundant transition metal nitrides as promising catalysts for NH_3 synthesis.

AUTHOR INFORMATION

Corresponding Author

*E-mail: chaowang@jhu.edu; bbukows1@jhu.edu.

Author Contributions

‡W.Q. and P. R. contributed equally to this work.

Notes

The authors declare no competing financial interest.

ASSOCIATED CONTENT

Supporting Information.
Experimental details, characterization data, and theoretical details.

ACKNOWLEDGMENT

This work was supported by the U.S. Department of Energy, Office of Science, Office of Basic Energy Sciences, Division of Chemical Sciences, Geosciences and Biosciences under Award No. DE-SC0023403. This research used resources of the National Energy Research Scientific Computing Center (NERSC), a Department of Energy Office of Science User Facility using NERSC award BES-ERCAP0027946. We acknowledge Materials Characterization and Processing (MCP) at Johns Hopkins University for the facilities. We thank Yuchen Niu from the Surface Analysis Center (SAC) at the University of Maryland for the help in the XPS measurements.

REFERENCES

(1) Erisman, J. W.; Sutton, M. A.; Galloway, J.; Klimont, Z.; Winiwarter, W. How a century of ammonia synthesis changed the world. *Nat. Geosci.* **2008,** *1*, 636–639.
(2) Schlögl, R. Catalytic synthesis of ammonia—a "never-ending story"? *Angew. Chem. Int. Ed.* **2003,** *42*, 2004–2008.
(3) Guo, J.; Chen, P. Catalyst: NH_3 as an energy carrier. *Chem* **2017,** *3*, 709–712.
(4) He, T.; Pachfule, P.; Wu, H.; Xu, Q.; Chen, P. Hydrogen carriers. *Nat. Rev. Mater.* **2016,** *1*, 16059.
(5) Smith, C.; Hill, A. K.; Torrente-Murciano, L. Current and future role of Haber–Bosch ammonia in a carbon-free energy landscape. *Energy Environ. Sci.* **2020,** *13*, 331–344.
(6) Chang, F.; Tezsevin, I.; de Rijk, J. W.; Meeldijk, J. D.; Hofmann, J. P.; Er, S.; Ngene, P.; de Jongh, P. E. Potassium hydride-intercalated graphite as an efficient heterogeneous catalyst for ammonia synthesis. *Nat. Catal.* **2022,** *5*, 222–230.
(7) Nawaz, M. A.; Blay-Roger, R.; Saif, M.; Meng, F.; González-Arias, J.; Miao, B.; Bobadilla, L. F.; Ramirez-Reina, T.; Odriozola, J. A. Enroute to the carbon-neutrality goals via the targeted development of ammonia as a potential nitrogen-based energy carrier. *ACS Catal.* **2023,** *13*, 14415–14453.
(8) Ye, D.; Tsang, S. C. E. Prospects and challenges of green ammonia synthesis. *Nat. Synth.* **2023,** *2*, 612–623.
(9) Ravi, M.; Makepeace, J. W. Facilitating green ammonia manufacture under milder conditions: what do heterogeneous catalyst formulations have to offer? *Chem. Sci.* **2022,** *13*, 890–908.
(10) Ye, T.-N.; Park, S.-W.; Lu, Y.; Li, J.; Sasase, M.; Kitano, M.; Tada, T.; Hosono, H. Vacancy-enabled N_2 activation for ammonia synthesis on an Ni-loaded catalyst. *Nature* **2020,** *583*, 391–395.
(11) Wang, P.; Chang, F.; Gao, W.; Guo, J.; Wu, G.; He, T.; Chen, P. Breaking scaling relations to achieve low-temperature ammonia synthesis through LiH-mediated nitrogen transfer and hydrogenation. *Nat. Chem.* **2017,** *9*, 64–70.
(12) Jacobsen, C. J. H.; Dahl, S.; Clausen, B. S.; Bahn, S.; Logadottir, A.; Nørskov, J. K. Catalyst design by interpolation in the periodic table: Bimetallic ammonia synthesis catalysts. *J. Am. Chem. Soc.* **2001,** *123*, 8404–8405.
(13) Jacobsen, C. J. H.; Dahl, S.; Hansen, P. L.; Törnqvist, E.; Jensen, L.; Topsøe, H.; Prip, D. V.; Møenshaug, P. B.; Chorkendorff, I. Structure sensitivity of supported ruthenium catalysts for ammonia synthesis. *J. Mol. Catal. A-Chem* **2000,** *163*, 19–26.
(14) Honkala, K.; Hellman, A.; Remediakis, I. N.; Logadottir, A.; Carlsson, A.; Dahl, S.; Christensen, C. H.; Nørskov, J. K. Ammonia synthesis from first-principles calculations. *Science* **2005,** *307*, 555–558.
(15) Ye, T.-N.; Park, S.-W.; Lu, Y.; Li, J.; Sasase, M.; Kitano, M.; Hosono, H. Contribution of nitrogen vacancies to ammonia synthesis over metal nitride catalysts. *J. Am. Chem. Soc.* **2020,** *142*, 14374–14383.
(16) Ye, T.-N.; Park, S.-W.; Lu, Y.; Li, J.; Wu, J.; Sasase, M.; Kitano, M.; Hosono, H. Dissociative and associative concerted mechanism for ammonia synthesis over Co-based catalyst. *J. Am. Chem. Soc.* **2021,** *143*, 12857–12866.
(17) van der Ham, C. J. M.; Koper, M. T. M.; Hetterscheid, D. G. H. Challenges in reduction of dinitrogen by proton and electron transfer. *Chem. Soc. Rev.* **2014,** *43*, 5183–5191.
(18) Widenmeyer, M.; Hansen, T. C.; Leineweber, A.; Weidenkaff, A.; Niewa, R. Nitrogen transfer between solid phases in the system Mn-N detected via in situ neutron diffraction. *Z. anorg. allg. Chem.* **2017,** *643*, 1929–1938.
(19) Feng, S.; Gao, W.; Wang, Q.; Guan, Y.; Yan, H.; Wu, H.; Cao, H.; Guo, J.; Chen, P. A multi-functional composite nitrogen carrier for ammonia production via a chemical looping route. *J. Mater. Chem. A* **2021,** *9*, 1039–1047.
(20) Michalsky, R.; Avram, A. M.; Peterson, B. A.; Pfromm, P. H.; Peterson, A. A. Chemical looping of metal nitride catalysts: low-pressure ammonia synthesis for energy storage. *Chem. Sci.* **2015,** *6*, 3965–3974.
(21) Laassiri, S.; Zeinalipour-Yazdi, C. D.; Catlow, C. R. A.; Hargreaves, J. S. J. The potential of manganese nitride based materials as nitrogen transfer reagents for nitrogen chemical looping. *Appl. Catal. B* **2018,** *223*, 60–66.
(22) Chang, F.; Guan, Y.; Chang, X.; Guo, J.; Wang, P.; Gao, W.; Wu, G.; Zheng, J.; Li, X.; Chen, P. Alkali and alkaline earth hydrides-driven N_2 activation and transformation over Mn nitride catalyst. *J. Am. Chem. Soc.* **2018,** *140*, 14799–14806.
(23) Leineweber, A.; Jacobs, H.; Kockelmann, W. Nitrogen ordering in ζ-manganese nitrides with hcp arrangement of Mn – MnN_y with $0.39 < y < 0.48$ – determined by neutron diffraction. *J. Alloys Compd.* **2004,** *368*, 229–247.
(24) Niewa, R. Nitridocompounds of manganese: manganese nitrides and nitridomanganates. *Z. Kristallogr.* **2002,** *217*, 8-23.
(25) Lu, Y.; Ye, T.-N.; Li, J.; Li, Z.; Guan, H.; Sasase, M.; Niwa, Y.; Abe, H.; Li, Q.; Pan, F.; Kitano, M.; Hosono, H. Approach to chemically durable nickel and cobalt lanthanum-nitride-based catalysts for ammonia synthesis. *Angew. Chem. Int. Ed.* **2022,** *61*, e202211759.
(26) Hu, Y.; Li, C.; Xi, S.; Deng, Z.; Liu, X.; Cheetham, A. K.; Wang, J. Direct pyrolysis of a manganese-triazolate metal–organic framework into air-stable manganese nitride nanoparticles. *Adv. Sci.* **2021,** *8*, 2003212.
(27) Milke, B.; Wall, C.; Metzke, S.; Clavel, G.; Fichtner, M.; Giordano, C. A simple synthesis of $MnN_{0.43}$@C nanocomposite: characterization and application as battery material. *J. Nanopart. Res.* **2014,** *16*, 2795.
(28) Iriawan, H.; Andersen, S. Z.; Zhang, X.; Comer, B. M.; Barrio, J.; Chen, P.; Medford, A. J.; Stephens, I. E. L.; Chorkendorff, I.; Shao-Horn, Y. Methods for nitrogen activation by reduction and oxidation. *Nat. Rev. Methods Primers* **2021,** *1*, 56.
(29) Walter, C.; Menezes, P. W.; Orthmann, S.; Schuch, J.; Connor, P.; Kaiser, B.; Lerch, M.; Driess, M. A molecular approach to manganese nitride acting as a high performance electrocatalyst

in the oxygen evolution reaction. *Angew. Chem. Int. Ed.* **2018,** *57*, 698–702.
(30) Burnett, J. A.; Allgood, H. Y.; Hall, J. R. Stabilization of ammonia synthesis catalyst. *Ind. Eng. Chem.* **1953,** *45*, 1678–1682.
(31) Andersen, S. Z.; Čolić, V.; Yang, S.; Schwalbe, J. A.; Nielander, A. C.; McEnaney, J. M.; Enemark-Rasmussen, K.; Baker, J. G.; Singh, A. R.; Rohr, B. A.; Statt, M. J.; Blair, S. J.; Mezzavilla, S.; Kibsgaard, J.; Vesborg, P. C. K.; Cargnello, M.; Bent, S. F.; Jaramillo, T. F.; Stephens, I. E. L.; Nørskov, J. K.; Chorkendorff, I. A rigorous electrochemical ammonia synthesis protocol with quantitative isotope measurements. *Nature* **2019,** *570*, 504–508.
(32) Aika, K.; Kumasaka, M.; Oma, T.; Kato, O.; Matsuda, H.; Watanabe, N.; Yamazaki, K.; Ozaki, A.; Onishi, T. Support and promoter effect of ruthenium catalyst. III. Kinetics of ammonia synthesis over various Ru catalysts. *Appl. Catal.* **1986,** *28*, 57–68.
(33) Wu, S.; Peng, Y.-K.; Chen, T.-Y.; Mo, J.; Large, A.; McPherson, I.; Chou, H.-L.; Wilkinson, I.; Venturini, F.; Grinter, D.; Ferrer Escorihuela, P.; Held, G.; Tsang, S. C. E. Removal of hydrogen poisoning by electrostatically polar MgO support for low-pressure NH_3 synthesis at a high rate over the Ru catalyst. *ACS Catal.* **2020,** *10*, 5614–5622.
(34) Hagen, S.; Barfod, R.; Fehrmann, R.; Jacobsen, C. J. H.; Teunissen, H. T.; Chorkendorff, I. Ammonia synthesis with barium-promoted iron–cobalt alloys supported on carbon. *J. Catal.* **2003,** *214*, 327–335.
(35) Urabe, K.; Aika, K.-I.; Ozaki, A. Activation of nitrogen by alkali metal-promoted transition metal: VI. Hydrogen effect on isotopic equilibration of nitrogen and rate-determining step of ammonia synthesis on potassium-promoted ruthenium catalysts. *J. Catal.* **1976,** *42*, 197–204.
(36) Kitano, M.; Kanbara, S.; Inoue, Y.; Kuganathan, N.; Sushko, P. V.; Yokoyama, T.; Hara, M.; Hosono, H. Electride support boosts nitrogen dissociation over ruthenium catalyst and shifts the bottleneck in ammonia synthesis. *Nat. Commun.* **2015,** *6*, 6731.
(37) Liu, Y.; Xu, L.; Li, X.; Hu, P.; Li, S. Growth and magnetic property of ζ-phase $Mn_2N_{1\pm x}$ thin films by plasma-assisted molecular beam epitaxy. *J. Appl. Phys.* **2010,** *107*, 103914.
(38) Meng, M.; Wu, S. X.; Ren, L. Z.; Zhou, W. Q.; Wang, Y. J.; Wang, G. L.; Li, S. W. Enlarged Mn 3*s* splitting and room-temperature ferromagnetism in epitaxially grown oxygen doped $Mn_2N_{0.86}$ films. *J. Appl. Phys.* **2014,** *116*, 173911.
(39) Selvaraju, V.; Brady-Boyd, A.; O'Connor, R.; Hughes, G.; Bogan, J. Investigation of nitrogen incorporation into manganese based copper diffusion barrier layers for future interconnect applications. *Surf. Interfaces* **2018,** *13*, 133–138.
(40) Ning, S.; Xu, H.; Qi, Y.; Song, L.; Zhang, Q.; Ouyang, S.; Ye, J. Microstructure induced thermodynamic and kinetic modulation to enhance CO_2 photothermal reduction: A case of atomic-scale dispersed Co–N species anchored Co@C hybrid. *ACS Catal.* **2020,** *10*, 4726–4736.
(41) Jin, H.; Li, L.; Liu, X.; Tang, C.; Xu, W.; Chen, S.; Song, L.; Zheng, Y.; Qiao, S.-Z. Nitrogen vacancies on 2D layered W_2N_3: A stable and efficient active site for nitrogen reduction reaction. *Adv. Mater.* **2019,** *31*, 1902709.
(42) Luo, S.; Liu, Y.; Song, Y.; Yang, Y.; Chen, F.; Chen, S.; Wei, Z. Plasma-induced nitrogen vacancy-mediated ammonia synthesis over a VN catalyst. *Chem. Commun.* **2024,** *60*, 3295–3298.
(43) Chen, Z.; Wu, R.; Liu, Y.; Ha, Y.; Guo, Y.; Sun, D.; Liu, M.; Fang, F. Ultrafine Co Nanoparticles Encapsulated in Carbon-Nanotubes-Grafted Graphene Sheets as Advanced Electrocatalysts for the Hydrogen Evolution Reaction. *Adv. Mater.* **2018,** *30*, 1802011.
(44) Niewa, R.; Hu, Z.; Kniep, R. Mn and Fe K-edge XAS Spectra of Manganese and Iron Nitrido Compounds. *Eur. J. Inorg. Chem.* **2003,** *2003*, 1632–1634.
(45) Miura, A.; Rosero-Navarro, C.; Masubuchi, Y.; Higuchi, M.; Kikkawa, S.; Tadanaga, K. Nitrogen-Rich Manganese Oxynitrides with Enhanced Catalytic Activity in the Oxygen Reduction Reaction. *Angew. Chem. Int. Ed.* **2016,** *55*, 7963–7967.

SYNOPSIS TOC

Insert Table of Contents artwork here